Magnetic reconnection and modification of the Hall physics due to cold ions at the magnetopause.

M. André[1], W. Li[1], S. Toledo-Redondo[2], Yu. V. Khotyaintsev[1], A. Vaivads[1],
D. B. Graham[1], C. Norgren[1], J. Burch[3], P.-A. Lindqvist[4], G. Marklund[4], R. Ergun[5], R. Torbert[3,6],
W. Magnes[7], C. T. Russell[8], B. Giles[9], T. E. Moore[9],
M. O. Chandler[10], C. Pollock[9,11], D. T. Young[3], L. A. Avanov[9], J. C. Dorelli[9], D. J. Gershman[9,12],
W. R. Paterson[9], B. Lavraud[13,14], Y. Saito[15]

[1]Swedish Institute of Space Physics, Uppsala, Sweden
[2]European Space Agency ESAC, Madrid, Spain
[3]Southwest Research Institute, San Antonio, USA
[4]KTH, Stockholm, Sweden
[5]LASP, University of Colorado, USA
[6]University of New Hampshire, USA
[7]Space Research Institute, Austrian Academy of Science, Austria
[8]UCLA, USA
[9]NASA Goddard Space Flight Center, USA
[10]NASA Marshall Space Flight Center, USA
[11]Denali Scientific, USA
[12]University of Maryland, College Park, MD, USA
[13]Institut de Recherche en Astrophysique et Planétologie, Université de Toulouse, France
[14]Centre National de la Recherche Scientifique, UMR 5277, Toulouse, France
[15]JAXA, Japan

Corresponding author: M. André, Swedish Institute of Space Physics, Box 537,
SE 751 21 Uppsala, Sweden. (mats.andre@irfu.se)

Key points:

Verification at high resolution that cold ions introduce a new length-scale at the magnetopause.

Verification at high resolution that cold ions modify the Hall physics of magnetic reconnection and reduce Hall currents.

Separatrix normal electric field balanced by the Hall term, the cold ion term, and the divergence of the electron pressure tensor.

AGU index terms:
2712 Electric fields
2723 Magnetic reconnection
2724 Magnetopause and boundary layers
7845 Particle acceleration
7855 Spacecraft sheaths, wakes, charging

Abstract

Observations by the four Magnetospheric Multiscale spacecraft are used to investigate the Hall physics of a magnetopause magnetic reconnection separatrix layer. Inside this layer of currents and strong normal electric fields, cold (eV) ions of ionospheric origin can remain frozen-in together with the electrons. The cold ions reduce the Hall current.
Using a generalized Ohm´s law, the electric field is balanced by the sum of the terms corresponding to the Hall current, the **vxB** drifting cold ions, and the divergence of the electron pressure tensor. A mixture of hot and cold ions is common at the subsolar magnetopause. A mixture of length-scales caused by a mixture of ion temperatures has significant effects on the Hall physics of magnetic reconnection.

Introduction

Magnetic reconnection is a process whereby microscopic plasma processes cause macroscopic changes in magnetic topology. Initially separated plasma regions become magnetically connected and energy stored in magnetic fields is converted into kinetic energy of charged particles (*Priest and Forbes*, 2000; *Fujimoto et al*., 2011). Reconnection is important in magnetospheric physics for solar wind entry and coupling (*Paschmann et al.,* 2013; *Phan et al*., 2015; *Hesse et al.,* 2015; *Burch et al.,* 2016), in several astrophysical environments (*Cassak et al.,* 2008; *Goodman and Uzdensky*, 2008; *Drake et al.,* 2010) and is regarded as one of the major obstacles for reaching plasma confinement in fusion and laboratory plasma devices (*Koepke*, 2008; *Moser and Bellan*, 2012).

For reconnection to occur, the MHD "frozen-in" condition must break down in the thin current sheet separating two plasma regions. In somewhat wider regions some particles with small enough gyroradii can be frozen-in (typically electrons) while particles with larger gyroradii can not fit inside the region (typically ions). Reconnection can be studied in detail at Earth´s magnetopause using the four Magnetospheric Multiscale (MMS) spacecraft (*Burch et al.,* 2015; *Fuselier et al.,* 2015). Here ion distributions with different temperatures and gyroradii are present, introducing multiple length-scales. Magnetosheath and hot magnetospheric ions have energies from a few hundred eV to several keV. Additional low-energy (few eV) positive ions of ionospheric origin are often present as well. Such ions are known to exist in the magnetosphere (*Chappell et al*., 1980; 1987; *Moore et al.,* 1997; *Cully et al.,* 2003) but are hard to detect onboard a spacecraft in a low-density plasma. The spacecraft can be positively charged to several tens of volts due to photoelectron emission, preventing the ions from reaching onboard detectors. A technique based on the detection of the wake behind a charged spacecraft in a supersonic ion flow has been developed to detect low-energy ions (*Engwall et al.,* 2009; *André et al*., 2015). A statistical study using this "wake method" and other techniques shows that cold ions are present about 90% of the time just inside the subsolar magnetopause (*André and Cully*, 2012). Here a "wind" and higher density "plumes" from the plasmasphere contribute plasma of ionospheric ions (*Darrouzet et al*., 2008; *Dandouras*, 2013; *Walsh et al.*, 2014a). However, most previous studies of reconnection at the magnetopause, including simulation studies, do not consider cold ions (*Cassak and Shay*, 2007; *Birn et al.*, 2008; *Pritchett and Mozer*, 2009). Cold ion plumes can increase the density and decrease the Alfvén velocity, and hence decrease the reconnection rate (*Walsh et al.*, 2014b). In addition, physics at the scale of the gyro radius and shorter (microphysics) is modified by the presence of cold ions.

In the ion diffusion region, ions are demagnetized while the electrons remain magnetized and carry so-called Hall currents. In separatrix regions, separating the inflow and outflow plasmas and extending away from the X-line, the situation is similar. Numerical simulations using one ion population predict a strong electric field normal to the magnetopause separatrix layer (*Pritchett and Mozer*, 2009; *Pritchett*, 2013). At high magnetopause latitudes, where cold ions are not so common, observations by the four Cluster satellites show that this electric field is balanced mainly by the Hall term (**j**x**B**)/(e n), i.e.by **E**x**B** drifting electrons (*André et al.*, 2004; *Retinò et al.*, 2006; *Khotyaintsev et al.*, 2006). At low latitudes, cold ions are very common, have a smaller gyroradius than the hot magnetosheath and magnetospheric ions, and remain magnetized down to smaller spatial scales. The cold ions introduce a new length-scale between the often discussed ion and electron scales. This is somewhat similar to the larger scale introduced by heavy ions (*Shay*

and Swisdak, 2004; *Markidis et al.*, 2011). In a separatrix region, the cold ions can **ExB** drift together with electrons and reduce the Hall currents. This scenario is consistent with observations by the Cluster spacecraft (*André et al.*, 2010, *Toledo-Redondo et al.*, 2015; 2016). We present MMS observations at much higher resolution (*Burch et al*., 2015). The physics at these scales is relevant for particle energization and the reconnection rate (*Drake et al*., 2008; *Yamada et al.*, 2010; *Liu et al.*, 2014).

Generalized Ohm´s law with cold ions

To study structures at scales between the ion and electron scales we use a generalized Ohm´s law including both ion and electron terms:

$$\mathbf{E} = (1/e\ n)(\mathbf{j}x\mathbf{B}) - 1/(e\ n)\ \mathrm{div}\ \mathbf{P_e} - (n_h/n)(\mathbf{v_h}x\mathbf{B}) - (n_m/n)(\mathbf{v_m}x\mathbf{B}) - (n_c/n)(\mathbf{v_c}x\mathbf{B}) \qquad (1)$$

neglecting time variations and the electron inertial term (valid for scales above the electron inertial length) (*Toledo-Redondo et al.*, 2015). Here **E** and **B** are the electric and magnetic fields, $\mathbf{P_e}$ is the electron pressure tensor, n_h, n_m and n_c are the densities of the hot, medium and cold ion populations, $n = n_h + n_m + n_c$ and the current is given by $\mathbf{j}=e(n_h\mathbf{v_h} + n_m\mathbf{v_m} + n_c\mathbf{v_c} - n\mathbf{v_e})$ where $\mathbf{v}_h$, $\mathbf{v}_m$, $\mathbf{v}_c$ and $\mathbf{v}_e$ are the velocities of the ion components and the electrons. At large (MHD) scales all fluids move together and equation (1) describes the frozen-in condition, while at scales below the cold ion gyroradius ρ_c all ion populations are demagnetized and localized electric fields must be supported by the first two terms on the right side of the equation. A new effect introduced by cold ions occurs at scales L, $\rho_c < L < \rho_m$. Here only cold ions and electrons are magnetized and the Hall term $(\mathbf{j}x\mathbf{B})/(e\ n)$ is partially cancelled by the cold ion term $(n_c/n)(\mathbf{v_c}x\mathbf{B})$ while other ions are not frozen-in.

Observations

We study the microphysics of reconnection and in particular the effects of cold ions in the separatrix region. We have searched MMS observations in the subsolar magnetopause region when the spacecraft are in a tetrahedron formation with a separation of about 10 km, and when burst mode data are available. We use data from the Fluxgate Magnetomer FGM (*Russell et al*., 2015), the Electric Double Probes EDP (*Lindqvist et al.*, 2015; *Ergun et al*., 2015) and the Fast Plasma Investigation FPI (*Pollock et al.*, 2016). As compared to previous Cluster studies (*André et al.*, 2010; *Toledo-Redondo et al*., 2015), the MMS configuration and detectors give many advantages since several assumptions in the data analysis can be removed. Four MMS spacecraft can be used for reliable velocity estimates of current sheets using timing (time differences of structures passing all spacecraft), and for estimates of currents from the curlometer technique (*Dunlop et al.*, 2002; *Russell et al*., 2015), and of the divergence of the pressure tensor, at the scale of the cold ion gyroradius. Previously one or two Cluster spacecraft and assumptions were used. Using MMS, electron and ion distributions can be obtained every 30 and 150 ms, respectively. Previously Cluster spacecraft potential and assumptions were used to obtain density at similar resolution (particle distributions were obtained at 4 s). Also, MMS has a 3D electric field instrument (including booms along the satellite spin axis) as opposed to the Cluster 2D

observations.

One event with clear signatures of reconnection was selected, including a narrow region likely to be a separatrix with a strong (> 10 mV/m) electric field and clear observations of cold ions. An overview of the selected event (2015-11-12) is shown in Fig.1 (upper part). The spacecraft location and separation are shown in Fig. 2a and b. MMS is moving from the magnetosheath, finally entering the magnetosphere around 06:19:20 UTC (Fig. 1, upper part). This is clear from the magnetic field becoming nearly northward (large B_z GSE (Geocentric Solar Ecliptic), panel a), the density decreasing (panel c) and the electron energy changing from around 100 eV to two components at tens of eV and a few keV (panel e). There are clear indications of a southward reconnection ion jet before entering the magnetosphere (v_z about -250 km/s, panel b, the predicted jet speed using parameters from the magnetosphere and the magnetosheath is 285 km/s, Cassak and Shay (2007)). The ion energy change from around a keV to two populations on the magnetospheric side, hot (several keV) and cold, panel d. The cold ions are cold in the sense that the thermal energy is tens of eV (verified by detailed studies of the ion distributions as discussed below) while the total energy can be a few 100 eV due to **E**x**B** drift. Hence these ions can reach the spacecraft and be directly detected (*Chandler et al.*, 1999; *Sauvaud et al.*, 2001; *Chandler and Moore*, 2003; *Chen and Moore*, 2004; 2006; *McFadden et al.*, 2008; *Lee and Angelopoulos*, 2014). (The spacecraft potential is about +5 V in the magnetosheath and about +15 V in the magnetosphere). The electric field X and Y components in GSE coordinates, essentially the components observed with the Spin Double Probe SDP instrument with a probe-to-probe separation of 120 m (*Lindqvist et al.*, 2015), are shown in panel f. Also displayed is the X component of the (**j**x**B**)/(e n) term in equation (1) (where **j** is estimated from the curlometer technique). This term is non-zero in the regions of strong electric fields indicating that not all particles are frozen in (ions and electrons move independently in the perpendicular direction) and can partly, but not fully, balance the normal electric field.

Figure 1, lower part, is similar to the upper part but for a shorter time interval and with the data shown in an LMN reference system. Using Minimum Variance Analysis applied to B (for the time period 06:19:02 to 06:19:23 UTC) the direction normal to the magnetopause N is estimated and is found to be approximately aligned with GSE X, consistent with the subsolar magnetopause region. The **L** direction is defined to be the maximum variance direction and **M** closes the system (see also caption of Fig. 1). The ion density is obtained for three energy intervals: hot, medium and cold (panel i). In panel j, cold ions can be easily identified after about 06:19:20.5 as a frozen-in **E**x**B** drifting population. As developed in the next paragraph, at earlier times more detailed analysis is needed to separate cold and magnetosheath ions. From about 06:19:20.0 magnetosheath ions can be observed only at increasingly higher energies (from a few hundred eV, later only above a keV). We interpret this as a finite gyroradius effect (ρ_m is about 100 km). Using Hot Plasma Composition Analyzer data (*Young et al.*, 2015) we find that most ions are protons, with the exception of some He^{2+} in the magnetosheath (not shown). While higher density plumes often include He^+ and O^+, a lower density cold plasma population may be mainly H^+ (*André and Cully*, 2012). The electric field components in panel l are obtained assuming **E**·**B**=0 (the MMS axial booms are not used for the final electric field in this varying plasma environment in this first investigation). The normal electric field E_N is larger than about 10 mV/m during about one second. Timing using four spacecraft, and the ion velocity in the normal direction, show that this region is moving roughly sunward at about 70-80 km/s, implying a separatrix region with a

width of about 70-100 km (see an approximate length-scale in Fig. 1). We investigate in detail which terms in equation (1) can balance this normal electric field.

Cold ions of ionospheric origin in the separatrix region have thermal energies of tens of eV but have drift energies of up to a few hundred eV. On the magnetospheric side the total cold ion energy is much lower than the hot magnetospheric ion energy (several keV), while on the magnetosheath side the total cold ion energy overlaps with the energy of shocked solar wind ions (Fig. 1). To determine the cold ion density, we use distributions in 3-dimensional ion velocity space (0.15 s time resolution). As cold ion density we use the total density in conical shaped regions in velocity space, from 100 eV up to 2 keV, approximately ± 45 degrees wide, centered on maximum differential particle flux of cold ions. On the magnetospheric side after 06:19: 21.0, this gives essentially the same result as integrating the density for all ion energies up to about 300 eV. For all times, the cold ion distributions are well separated in velocity space from the magnetosheath particles. Figure 3 shows examples of distributions when the densities of cold and medium energy ions are approximately equal (indicated by red bars in Fig. 1, panel j). Excluding bulk drift motion, these cold ion distributions have a temperature of about 50 eV. The cold ion drift determined from particle instruments agrees well with the **ExB** drift from electric and magnetic field observations. At higher energies, in our definition, hot (magnetospheric) ions have energies of 7-25 keV, and medium energy (magnetosheath) particles are all the remaining ions, with an average energy of about 0.8-1 keV, corresponding to gyroradii of 320 km and 100 km, respectively. The magnetosheath ions are not magnetized within the separatrix region (Fig. 3). Rather, these distributions are consistent with magnetosheath flow and a reconnection jet.

The terms in equation (1) are estimated using data from different instruments so we first compare the data sets. The four upper panels in Fig. 4 show the normal electric field from the four MMS spacecraft estimated in different ways. We have added 2 mV/m to the E_x (GSE, first using default calibration) EDP electric field to obtain better agreement with other estimates. The normal component E_N (using $\mathbf{E}\cdot\mathbf{B}=0$) is shown together with $-(\mathbf{v_c}\times\mathbf{B})$ and $-(\mathbf{v_e}\times\mathbf{B})$. When the electrons and cold ions are frozen in, all three estimates should agree. Since the gyroradii of cold ions and electrons are around 25 km and 1 km, respectively, and the region with strong E_N is about 70-100 km wide, all estimates should be similar. In the region of strong electric fields (> 10 mV/m), about 06:19:20.0 to 21.0, on average all three estimates agree well, with the electron term typically slightly larger than the other terms. The estimate of the cold ion term is varying smoother than the other estimates. The time resolution (0.15 s) of the ion detectors is higher than on previous comparable missions but still lower than for the other simultaneous observations. Also, the ions have a gyroradius (about 25 km) and gyro period (1.3 s), longer than the spatial and temporal distance between data points, and can not follow changes in the electric field at high frequencies. The estimate of the cold ion velocity is not reliable when these ions are a small fraction of the total ion population in the higher density magnetosheath (before about 06:19:20.0 UTC). On the other hand, here the electron velocity is well determined and E_N agrees well with $-(\mathbf{v_e}\times\mathbf{B})$. For the whole intervall, the EDP E_N and electron term estimates (here both displayed with a resolution of 0.03 s) show rather detailed agreement. This includes short (about 0.1 s) and strong (> 20 mV/m) electric fields observed mainly on MMS 3 and 4. After the region of strong electric fields, entering the lower density magnetosphere, the ion and electron terms agree, on average. These electric fields estimated from particle and magnetic field observation are here slightly lower than the EDP estimate (1-2 mV/m). This can partly be due to a changing effective

SDP boom length due to lower density and longer Debye length. In conclusion we find that the EDP and electron term estimates in general agree well and that it is meaningful to compare EDP electric field observations and estimates of this field from particle moments.

To investigate which terms in equation (1) balance E_N, we plot all terms for all four spacecraft in the next four panels of Fig. 4. For each spacecraft, E_N is from the EDP instrument, E_c is the normal component of the $(n_c/n)(\mathbf{v_c x B})$ term and E_m and E_h are defined in a similar way for medium energy and hot ions. Note that this cold ion term is different from the upper panels since now the cold ion density (n_c/n) is included. In the Hall term $(\mathbf{j x B})/(e\ n)$ the current is estimated from the curlometer method, using magnetic field data from all four spacecraft, so this is an average over the volume defined by the spacecraft configuration (this term is the same in all four lower panels). Estimates of the currents using particle moments from individual spacecraft are more variable while for the cold ions an average over the gyroradius (roughly the spacecraft separation) is relevant. The divergence of the electron pressure tensor $1/(e\ n)$ div $\mathbf{P_e}$ is estimated from observations on all four spacecraft (this term is the same in all four lower panels). The MMS electron FPI instruments have high time resolution (*Pollock et al.,* 2016) and with the present tetrahedron configuration the divergence term can be directly estimated.

Overall the normal electric field E_N observed with the EDP double probe instrument (black line in Fig. 4) is in good agreement with the sum of the estimated terms on the right side of equation (1) (red dashed line). Thus, the generalized Ohm´s law in this form is a meaningful way to describe the electric field on the ion scale in the separatrix region. In this region with a strong electric field, roughly 06:19:20.0 to 21.0, not all ions are frozen-in. This is seen by the Hall $(\mathbf{j x B})/(e\ n)$ term being non-zero (not all particles are moving together in the perpendicular direction). Early in the separatrix (on the magnetosheath side) the Hall term can balance E_N, but is then decreasing towards the lower density magnetosphere. Considering the terms including ion moments, E_m and E_h corresponding to medium and hot ion energies, are close to zero on all spacecraft. This is consistent with typical gyroradii at these energies, 100 and 320 km, wider than the separatrix region, so these ions are not frozen-in. (For the highest energy ions in this study, tens of keV, the width of the instrument energy channels is similar to the expected drift energy, hundreds of eV, making drifts hard to determine. However, these ions certainly have a gyroradius larger than the width of the separatrix.) The cold ion term in equation (1), E_c, is small before the spacecraft enter the strong electric field, before about 06:19:20.0 UTC, due to the relatively small cold ion density. After this time, the cold ion term is reliable and gradually increasing. Comparing the Hall and cold ion terms, our interpretation is that both electrons and cold ions (with a gyroradius of 1 and 25 km, respectively) **ExB** drift together inside the separatrix region, Fig. 2c. The cold ion density gradually becomes a larger fraction of the total density meaning that these ions gradually reduce a larger fraction of the Hall current. The Hall and cold ion terms become roughly equally important when the cold ion density is about half the total ion density (about 06:19:20.7 to 21.0). At the end of this short interval the divergence of the electron pressure tensor gives a significant contribution, 2-3 mV/m, all three terms summing up to about 10 mV/m. For comparison, in the lowest panel in Fig. 4 all observations are averaged over all four spacecraft. Here the EDP electric field, **vxB**, **jxB** and the divergence of the electron pressure tensor, all have similar spatial resolution. These detailed observations show how E_N in a separatrix region can be balanced by a sum of Hall $(\mathbf{j x B})/(e\ n)$ and cold ion $(n_c/n)(\mathbf{v_c x B})$ terms (representing frozen-in electrons and cold ions) and a term including the divergence of the

electron pressure tensor. We observe how the relative importance of these terms gradually varies as the relative density of cold ions varies.

Summary and Conclusion

We use high resolution observations by the four MMS spacecraft at the magnetopause to investigate the Hall physics of a reconnection separatrix layer. The separatrix is about 70-100 km wide, roughly the size of the magnetosheath (0.8-1 keV) ion gyroradius. Inside this layer cold (tens of eV) ions of ionospheric origin with smaller gyroradius can **E**x**B** drift together with electrons. The drifting ions reduce the Hall current. We speculate that a reduced current may change the instabilities in a separatrix. The normal electric field is balanced by the frozen-in particles (electrons carrying the Hall current and cold ions), together with the divergence of the electron pressure tensor, in regions where other particles (hotter ions) are not frozen in. This can be described by a generalized Ohm´s law including multiple ion components. We observe how the relative importance of the Hall and cold ion terms change as the relative density of cold ion varies within a separatrix.

A mixture of hot and cold ions is common at the subsolar magnetopause. A mixture of ion temperatures and scale lengths is probably common in many astroplasmas. A mixture of length-scales caused by a mixture of ion temperatures has significant effects on the Hall physics of magnetic reconnection.

Acknowledgements: We thank the entire MMS team and instrument PIs for data access and support. MMS data are available at https://lasp.colorado.edu/mms/sdc/public/. We acknowledge support from the Swedish National Space Board contracts SNSB 139/12, 164/14 and 176/15. The IRAP contribution to MMS was supported by CNES.

Figure 1
MMS 1 magnetopause crossing. (a) Magnetic field in GSE coordinates; (b) and (c) Ion velocities and density; (d) Ion differential energy flux and average energy obtained in the perpendicular direction; (e) Electron differential energy flux and spacecraft potential; (f) Electric field and X-component of the Hall term; (g) magnetic field in LMN coordinates (in GSE: L = [0.41, -0.63, 0.66]; M = [0.03, -0.72, -0.70]; N = [0.91, 0.31, -0.28]); (h) Ion velocity; (i) Ion densities for three energy levels, cold (n_c), medium (n_m) and hot (n_h), and the total density n; (j) Ion differential energy flux, average energy obtained in the perpendicular direction, and energy corresponding to **ExB** drift of protons (k) Electron differential energy flux and spacecraft potential; (l) Electric field. The spacecraft is crossing a separatrix region with a large E_N where not all particles are frozen-in: significant Hall term, panel f, and average (perpendicular) ion energy not corresponding to **ExB** drift energy, panel j.

Figure 2
Subsolar magnetopause crossing. (a) Location of the MMS spacecraft in the GSE X-Z plane. (b) Three-dimensional configuration of the MMS spacecraft. (c) Illustration of the separatrix region with a large normal electric field E_N and the gyroradii of hot (magnetospheric), medium energy (magnetosheath) and cold (ionospheric origin) positive ions, and electrons. Only cold ions and electrons remain magnetized in the region of large E_N.

Figure 3
Separatrix region ions. Differential ion flux (1/(cm^2 s sr keV)) in the direction parallel to **B** versus the perpendicular **ExB** direction (determined from field observations, corresponding velocity given by red circle), averaged over ± 30 degrees in the second perpendicular direction (time resolution: 0.15 s). Two examples show frozen-in **ExB** drifting cold ions, together with magnetosheath ions at higher energies.

Figure 4
Electric field and the generalized Ohm´s law. Upper four panels, for each spacecraft: Normal component of the electric field from the EDP instrument (E_N), and from the cold ion and electron drifts (-(**v_cxB)** and **-(v_exB)**). Next four panels, for each spacecraft: E_N as in the upper panels, the Hall term (1/e n)(**jxB**), the ion drift terms -(**vxB)** in equation (1) including the relative density of cold, medium and hot ions (E_c, E_m, E_h) and the divergence of the electron pressure tensor (E_{eP}) from the same equation. The lowest panel is similar to the middle panels, but all observations are averaged over all four spacecraft. The upper panels show in general good agreement between direct and indirect electric field estimates. The lower panels show that E_N is balanced by a combination of the Hall term, **ExB** drifting cold ions, and the divergence of E_{eP}.

References

André, M., K. Li, and A. I. Eriksson (2015), Outflow of low-energy ions and the solar cycle, *J. Geophys. Res. Space Physics*, 120, 1072–1085, doi:10.1002/ 2014JA020714.

André, M., A. Vaivads, Y. V. Khotyaintsev, T. Laitinen, H. Nilsson, G. Stenberg, A. Fazakerley, and J. G. Trotignon (2010), Magnetic reconnection and cold plasma at the magnetopause, *Geophys. Res. Lett.*, 37, L22108, doi:10.1029/2010GL044611.

André, M., and C. M. Cully (2012), Low-energy ions: A previously hidden solar system particle population, *Geophys. Res. Lett.*, 39, L03101, doi:10.1029/ 2011GL050242.

André, M., A. Vaivads, S. C. Buchert, A. Fazakerley, and A. Lahiff (2004), Thin electron-scale layers at the magnetopause, *Geophys. Res. Lett.*, *31*, L03803, doi:10.1029/2003GL018137.

Birn, J., J. Borovsky, and M. Hesse (2008), Properties of asymmetric magnetic reconnection, *Phys. Plasmas*, *15*(3), 032101.

Burch, J. L., et al. (2015), Magnetospheric Multiscale overview and science objectives, *Space Sci. Rev.*, doi:10.1007/s11214-015-0164-9.

Burch J. L. et al. (2016), Electron-Scale Measurements of Magnetic Reconnection in Space, in press, Science, doi:10.1126/science.aaf2939.

Cassak, P., and M. Shay (2007), Scaling of asymmetric magnetic reconnection: General theory and collisional simulations, *Phys. Plasmas*, 14(10), 102114.

Cassak, P. A., D. J. Mullan and M. A. Shay (2008), From solar and stellar flares to coronal heating: Theory and observations of how magnetic reconnection regulates coronal conditions, *Astrophys. J. Lett*., 676, L69, doi:10.1086/587055.

Chandler, M. O., et al. (1999), Evidence of component merging equatorward of the cusp, *J. Geophys. Res.*, 104, 22623-22633.

Chandler, M. O. and T. E. Moore (2003), Observations of the geopause at the equatorial magnetopause: Density and temperature, *Geophys. Res. Le*tt., 30, 1869, doi:10.1029/2003GL017611.

Chappell, C. R., C. R. Baugher, and J. L. Horwitz (1980), New advances in thermal plasma research, *Rev. Geophys*., 18, 853–861, doi:10.1029/RG018i004p00853.

Chappell, C. R., T. E. Moore, and J. H. Waite Jr. (1987), The ionosphere as a fully adequate source of plasma for the Earth's magnetosphere, *J. Geophys. Res*., 92, 5896–5910, doi:10.1029/JA092iA06p05896.

Chen, S.-H. and T. E. Moore (2004), Dayside flow bursts in the Earth's outer magnetosphere, *J. Geophys. Res.*, 109, A03215, doi:10.1029/2003JA010007.

Chen, S.-H. and T. E. Moore (2006), Magnetospheric convection and thermal ions in the dayside outer magnetosphere, *J. Geophys. Res*., 111, A03215, doi:10.1029/2005JA011084.

Cully, C. M., E. F. Donovan, A. W. Yau, and G. G. Arkos (2003), Akebono/Suprathermal Mass Spectrometer observations of low-energy ion outflow: Dependence on magnetic activity and solar wind conditions, *J. Geophys. Res.*, 108(A2), 1093, doi:10.1029/2001JA009200.

Dandouras, I. (2013), Detection of a plasmaspheric wind in the Earth's magnetosphere by the Cluster spacecraft, *Ann. Geophys.*, *31*, 1143 – 1153, doi:10.5194/angeo-31-1143-2013.

Darrouzet, F., J. D. Keyser, P. Décréau, F. E. Lemdani-Mazouz, and X. Vallières (2008), Statistical analysis of plasmaspheric plumes with Cluster/WHISPER observations, *Ann. Geophys.*, *26*, 2403–2417, doi:10.5194/angeo-26-2403-2008.

Drake, J. F. et al. (2010), A Magnetic reconnection mechanism for the generation of anomalous cosmic rays, *Astrophys. J*., 709, 963-974, doi:10.1088/0004-637X/709/2/963.

Drake, J. F., M. A. Shay, and M. Swisdak (2008), The Hall fields and fast magnetic reconnection, *Phys. Plasmas*, *15*(4), 042306, doi:10.1063/1.2901194.

Dunlop, M. W., et al. (2002), Four-point Cluster application of magnetic field analysis tools: The Curlometer, *J. Geophys. Res.*, 107(A11), 1384, doi:10.1029/2001JA005088.
Engwall, E., A. I. Eriksson, and J. Forest (2006), Wake formation behind positively charged spacecraft in flowing tenuous plasmas, *Phys. Plasmas*, 13, 062904, doi:10.1063/1.2199207.

Engwall, E., A. I. Eriksson, C. M. Cully, M. André, R. Torbert, and H. Vaith (2009), Earth's ionospheric outflow dominated by hidden cold plasma, *Nature Geosci.*, 2, 24–27, doi:10.1038/ngeo387.

Ergun, R. E., et al. (2015), The Axial Double Probe and Fields Signal Processing for the MMS Mission, *Space Sci. Rev*., doi:10.1007/s11214-014-0115-x.

Fujimoto, M., I. Shinohara and H. Kojima (2011), Reconnection and waves: A review with a perspective, *Space Sci. Rev.*, 160:123–143 doi:10.1007/s11214-011-9807-7.

Fuselier, S. A., et al. (2015), Magnetospheric Multiscale science mission profile and operations, *Space Sci. Rev*., doi:10.1007/s11214-014-0087-x.

Goodman, J. and D. Uzdensky (2008), Reconnection in marginally collisionless accretion disk coronae, *Astrophys. J.*, 688, 555, doi:10.1086/592345.

Hesse, M., et al. (2015), Theory and modeling for the Magnetospheric Multiscale mission, *Space Sci. Rev.*, doi:10.1007/s11214-014-0078-y.

Khotyaintsev, Y. V., A. Vaivads, A. Retinò, M. André, C. J. Owen, and H. Nilsson (2006), Formation of inner structure of a reconnection separatrix region, *Phys. Rev. Lett.*, *97*(20), 205003, doi:10.1103/PhysRevLett.97.205003.

Koepke, M. E. (2008), Interrelated laboratory and space plasma experiments, *Rev. Geophys.*, 46, RG3001, doi:10.1029/2005RG000168.

Lee, J. H., and V. Angelopoulos (2014), On the presence and properties of cold ions near Earth's equatorial magnetosphere, J. Geophys. Res. Space Physics, 119, 1749–1770, doi:10.1002/2013JA019305.

Lindqvist, P.-A., et al. (2015), The Spin-Plane Double Probe electric field instrument for MMS, *Space Sci. Rev.*, doi:10.1007/s11214-014-0116-9.

Liu, Y.-H., W. Daughton, H. Karimabadi, H. Li, and S. Peter Gary (2014), Do dispersive waves play a role in collisionless magnetic reconnection?, *Phys. Plasmas*, *21*(2), 022113, doi:10.1063/1.4865579.

Markidis, S., G. Lapenta, L. Bettarini, M. Goldman, D. Newman, and L. Andersson (2011), Kinetic simulations of magnetic reconnection in presence of a background O+ population, *J. Geophys. Res.*, *116*, A00K16, doi:10.1029/2011JA016429.

McFadden, J. P., et al. (2008), Structure of plasmaspheric plumes and their participation in magnetopause reconnection: First results from THEMIS, Geophys. Res. Lett., 35, L17S10, doi:10.1029/2008GL033677.

Moore, T. E., et al. (1997), High altitude observations of the polar wind, Science, 277, 349–351, doi:10.1126/science.277.5324.349.

Moser, A. L. and P. M. Bellan, Magnetic reconnection from a multiscale instability cascade, *Nature*, 482, 379-381, doi: 10.1038/nature10827, 2012.

Paschmann, G., M., M. Öieroset and T Phan (2013), In-situ observations of reconnection in space, *Space Sci. Rev.*, 178, 385-417, doi: 10.1007/s11214-012-9957-2.

Phan, T. D., et al. (2015), Establishing the context for reconnection diffusion region encounters

and strategies for the capture and transmission of diffusion region burst data by MMS, *Space Sci. Rev.*, doi:10.1007/s11214-015-0150-2.

Pollock, C., et al., (2016), Fast Plasma Investigation for Magnetospheric Multiscale, Space Sci. Rev., doi:10.1007/s11214-016-0245-4.

Priest, E. and T. Forbes, Magnetic reconnection (2000), Cambridge Univ. Press, Cambridge, ISBN 0-521-48179-1.

Pritchett, P., and F. Mozer (2009), Asymmetric magnetic reconnection in the presence of a guide field, *J. Geophys. Res.*, *114*, A11210, doi:10.1029/2009JA014343.

Pritchett, P. L. (2013), The influence of intense electric fields on three-dimensional asymmetric magnetic reconnection, *Phys. Plasmas*, *20*(6), 061204, doi:10.1063/1.4811123.

Russell, C. T., et al. (2015), The Magnetospheric Multiscale magnetometers, *Space Sci. Rev.*, doi:10.1007/s11214-014-0057-3.

Sauvaud, J.-A., et al. (2001), Intermittent thermal plasma acceleration linked to sporadic motions of the magnetopause, first Cluster results, *Ann. Geophys*., 19, 1523, doi:10.5194/angeo-19-1523-2001.

Shay, M. A., and M. Swisdak (2004), Three-species collisionless reconnection: Effect of O+ on magnetotail reconnection, *Phys. Rev. Lett.*, *93*(17), 175001, doi:10.1103/PhysRevLett.93.175001.

Toledo-Redondo, S., A. Vaivads, M. André, and Y. V. Khotyaintsev (2015), Modification of the Hall physics in magnetic reconnection due to cold ions at the Earth's magnetopause, *Geophys. Res. Lett.*, 42, 6146 – 6154, doi:10.1002/2015GL065129.

Toledo-Redondo, S., M. André, A. Vaivads, Yu. V. Khotyaintsev, B. Lavraud, D. B. Graham, A. Divin, and N. Aunai (2016), Cold ion heating at the dayside magnetopause during magnetic reconnection, *Geophys. Res. Lett.*, *43*, 58–66, doi:10.1002/2015GL067187.

Retinò, A., et al. (2006), Structure of the separatrix region close to a magnetic reconnection X-line: Cluster observations, *Geophys. Res. Lett.*, *33*, L06101, doi:10.1029/2005GL024650.

Walsh, B., J. Foster, P. Erickson, and D. Sibeck (2014a), Simultaneous ground- and space-based observations of the plasmaspheric plume and reconnection, *Science*, *343*(6175), 1122–1125.

Walsh, B., T. Phan, D. Sibeck, and V. Souza (2014b), The plasmaspheric plume and magnetopause reconnection, *Geophys. Res. Lett.*, *41*, 223–228, doi:10.1002/2013GL058802.

Yamada, M., R. Kulsrud, and H. Ji (2010), Magnetic reconnection, *Rev. Mod. Phys.*, *82*(1), 603, doi:10.1103/RevModPhys.82.603.

Young, D. T. (2015), Hot Plasma Composition Analyzer for the Magnetospheric Multiscale Mission, Space Sci. Rev., doi:10.1007/s11214-014-0119-6.

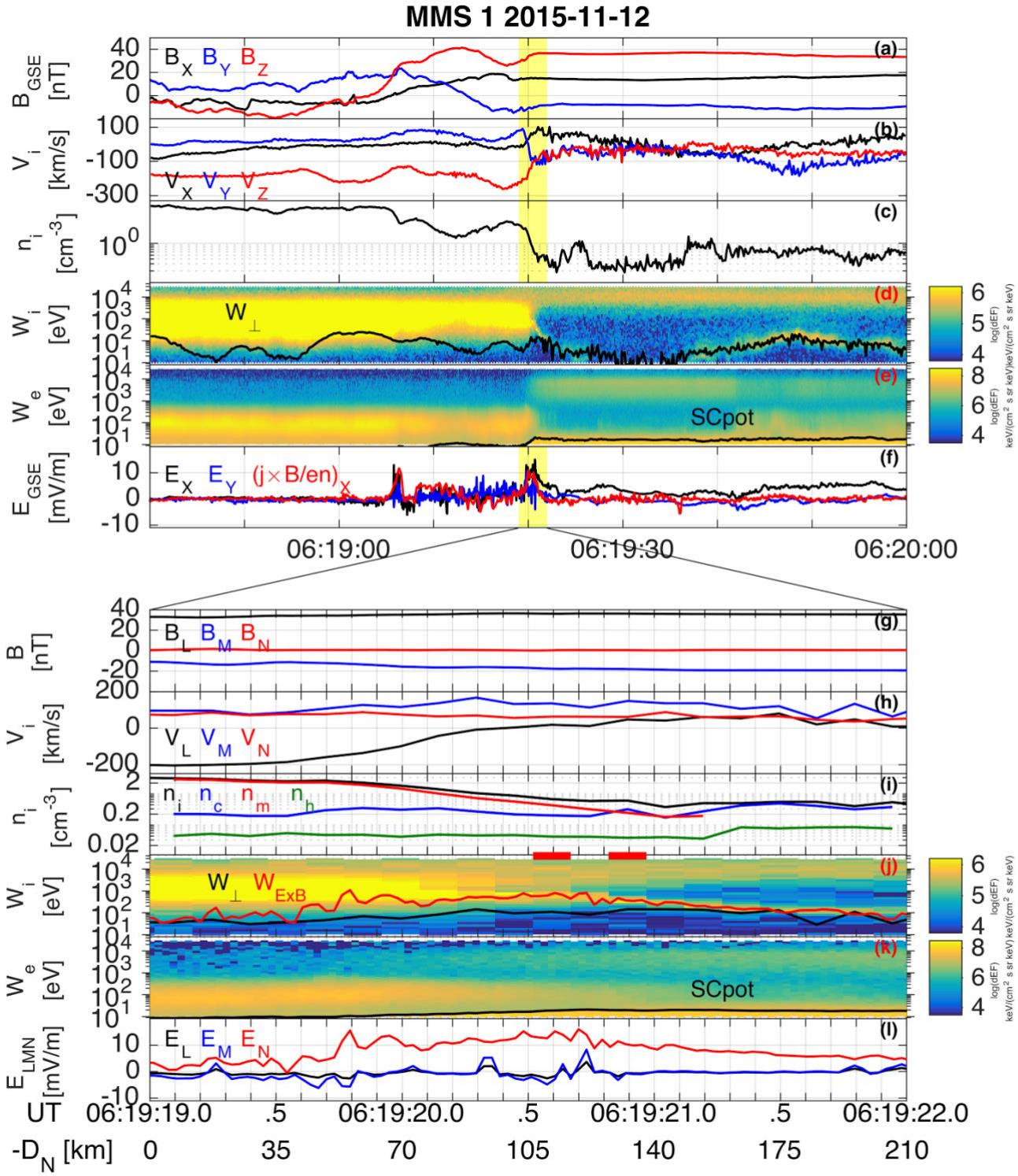
MMS 1 2015-11-12
B_GSE [nT]
B_X B_Y B_Z
(a)
V_i [km/s]
V_X V_Y V_Z
(b)
n_i [cm^-3]
(c)
W_i [eV]
W_⊥
(d)
W_e [eV]
SCpot
(e)
E_GSE [mV/m]
E_X E_Y (j×B/en)_X
(f)
06:19:00
06:19:30
06:20:00
B [nT]
B_L B_M B_N
(g)
V_i [km/s]
V_L V_M V_N
(h)
n_i [cm^-3]
n_i n_c n_m n_h
(i)
W_i [eV]
W_⊥ W_ExB
(j)
W_e [eV]
SCpot
(k)
E_LMN [mV/m]
E_L E_M E_N
(l)
log(dEF) keV/(cm^2 s sr keV)
UT
06:19:19.0
.5
06:19:20.0
.5
06:19:21.0
.5
06:19:22.0
-D_N [km]
0
35
70
105
140
175
210

Figure 1

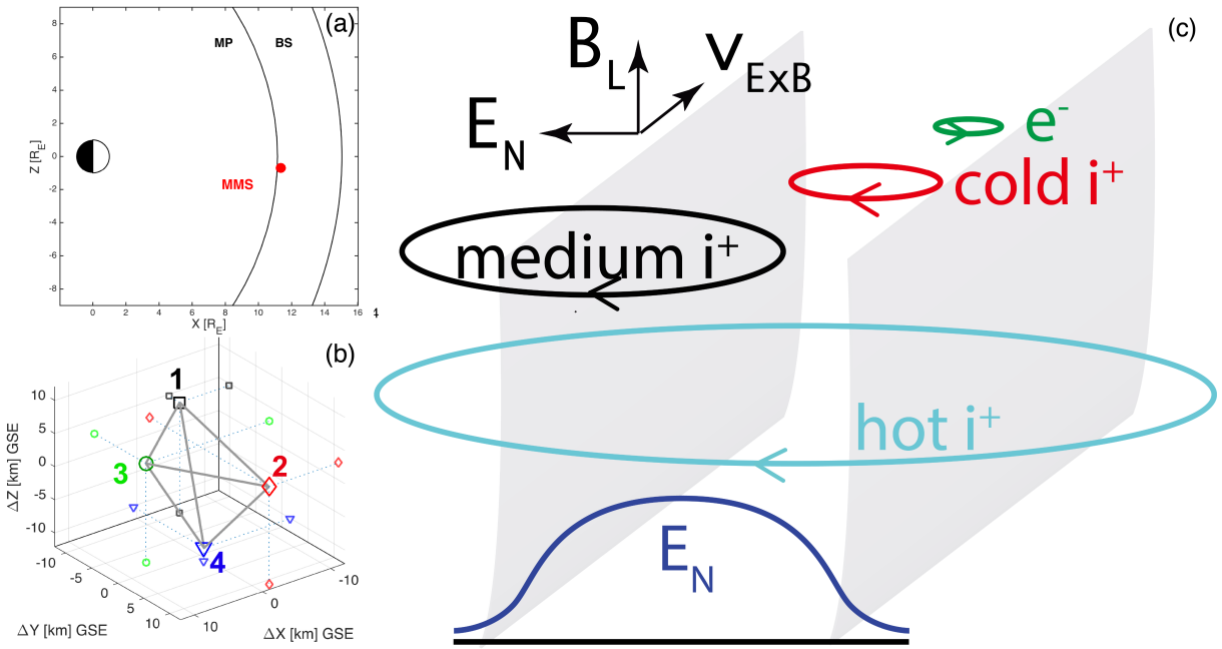
(a)
MP
BS
MMS
Z [R_E]
X [R_E]
(b)
1
2
3
4
ΔZ [km] GSE
ΔY [km] GSE
ΔX [km] GSE
(c)
B_L
v_ExB
E_N
e-
cold i+
medium i+
hot i+
E_N

Figure 2

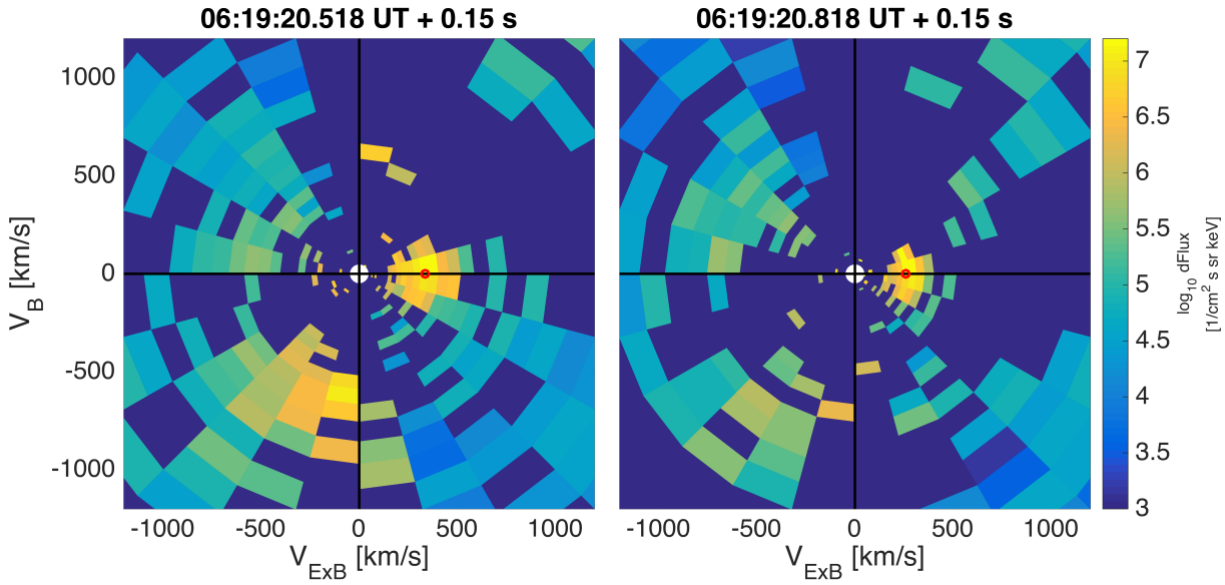
06:19:20.518 UT + 0.15 s
06:19:20.818 UT + 0.15 s
1000
500
0
-500
-1000
V_B [km/s]
-1000
-500
0
500
1000
V_ExB [km/s]
7
6.5
6
5.5
5
4.5
4
3.5
3
log10 dFlux
[1/cm2 s sr keV]

Figure 3

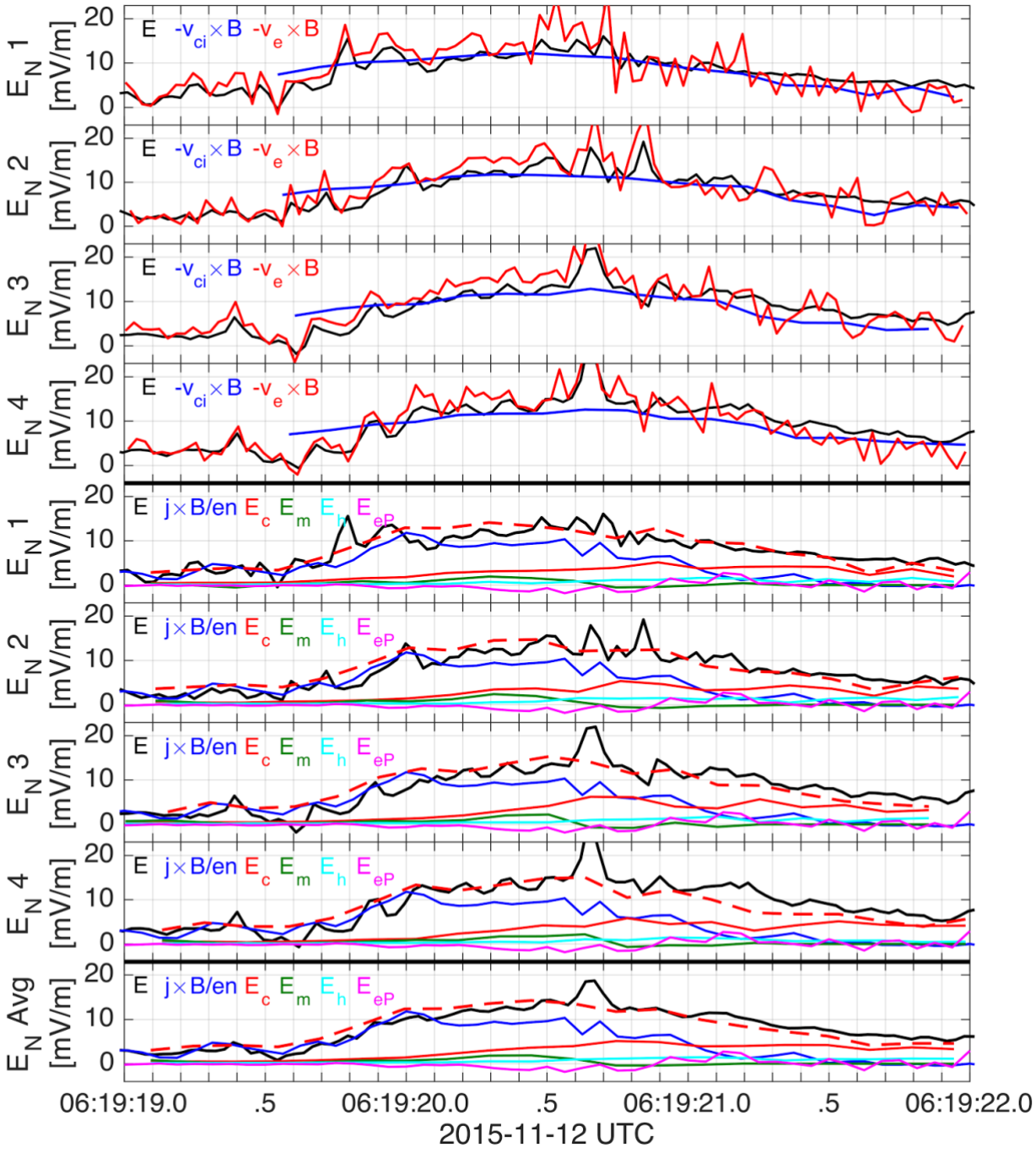
E -v_ci×B -v_e×B
E j×B/en E_c E_m E_h E_eP
E_N 1 [mV/m]
E_N 2 [mV/m]
E_N 3 [mV/m]
E_N 4 [mV/m]
E_N Avg [mV/m]
20
10
0
06:19:19.0
.5
06:19:20.0
.5
06:19:21.0
.5
06:19:22.0
2015-11-12 UTC

Figure 4